SCIENTIFIC REPORTS
nature research

OPEN

Bulk superconductivity in a four-layer-type Bi-based compound $La_2O_2Bi_3Ag_{0.6}Sn_{0.4}S_{5.7}Se_{0.3}$

Received: 13 May 2019
Accepted: 3 September 2019
Published online: 19 September 2019

Rajveer Jha[1], Yosuke Goto[1], Tatsuma D. Matsuda[1], Yuji Aoki[1], Masanori Nagao[2], Isao Tanaka[2] & Yoshikazu Mizuguchi[1]

Recently, we reported the observation of superconductivity at ~0.5 K in a $La_2O_2M_4S_6$-type (M: metal) layered compound $La_2O_2Bi_3AgS_6$, which is a layered system related to the BiS_2-based superconductor system but possesses a thicker Bi_3AgS_6-type conducting layer. In this study, we have developed the $La_2O_2Bi_3AgS_6$-type materials by element substitutions to increase the transition temperature (T_c) and to induce bulk nature of superconductivity. A resistivity anomaly observed at 180 K in $La_2O_2Bi_3AgS_6$ was systematically suppressed by Sn substitution for the Ag site. By the Sn substitution, T_c increased, and the shielding volume fraction estimated from magnetization measurements also increased. The highest T_c (=2.3 K) and the highest shielding volume fraction (~20%) was observed for $La_2O_2Bi_3Ag_{0.6}Sn_{0.4}S_6$. The superconducting properties were further improved by Se substitutions for the S site. By the combinational substitutions of Sn and Se, bulk-superconducting phase of $La_2O_2Bi_3Ag_{0.6}Sn_{0.4}S_{5.7}Se_{0.3}$ with a T_c of 3.0 K (T_c^{onset} = 3.6 K) was obtained.

Layered superconductors have been extensively studied due to observations of unconventional superconductivity and high transition temperature (T_c)[1,2]. In addition, the great flexibility of constituent elements and layered (stacking) structure, the studies on layered superconductor system can be widely developed. The recent discovery of BiS_2-based superconductors has also created remarkable attention in the superconductivity community: the typical materials are $Bi_4O_4S_3$, $REO_{1-x}F_xBiS_2$ (RE = La, Ce, Pr, Nd, Yb), and $Sr_{1-x}RE_xFBiS_2$[3–14]. For instance, the crystal structure of the typical system $LaOBiS_2$ is composed of alternate stacks of a La_2O_2 blocking layer and two BiS_2 layers. Since the parent phase ($LaOBiS_2$) is an insulator with a band gap[15], electron doping is needed to induce metallic and superconducting characteristics. Furthermore, local in-plane structure should be optimized to induce bulk superconductivity in the BiS_2 layer[16]. Thus, the T_c of BiS_2-based is sensitive to physical pressure[4,17–21] and chemical pressure[22–24] effects and reaches 11 K in $LaO_{0.5}F_{0.5}BiS_2$. Therefore, an increase in the highest record of T_c in the BiS_2-based superconductor family can be expected by further material development and tuning of structural and electrical properties[14].

Very recently, we reported on the superconductivity in oxychalcogenide $La_2O_2Bi_3AgS_6$ with T_c of 0.5 K[25]. The crystal structure of $La_2O_2Bi_3AgS_6$ is similar to the typical BiS_2-based superconductor $LaOBiS_2$, but the conducting layer thickness is thicker than that of $LaOBiS_2$. The crystal structure of the system can be described as $La_2O_2M_4S_6$, in which the M site can be Pb, Bi, and Ag[26–28]. There are two different metal sites [M1 and M2 displayed in Fig. 1(c)] in the M_4S_6-type conducting layer. For the outer layers with the M1 site, Bi selectively occupies, and the layers can be regarded as the BiS_2-type layers. For the inner layer with the M2 site, NaCl-type (Bi,Ag)S_2 layers are inserted in between the BiS_2-type layers.

Interestingly, an anomalous transport property was observed in the temperature dependence of resistivity in $La_2O_2Bi_3AgS_6$[25], which is similar to the charge-density-wave (CDW) transition in $EuFBiS_2$[29]. In this study, we have investigated the Sn substitution effect for the Ag site in $La_2O_2Bi_3Ag_{1-x}Sn_xS_6$ and found that the resistivity anomaly was suppressed by Sn substitutions. T_c reached 2.3 K for $x = 0.4$ ($La_2O_2Bi_3Ag_{0.6}Sn_{0.4}S_6$). Furthermore, by Se substitutions for the S site in $La_2O_2Bi_3Ag_{0.6}Sn_{0.4}S_{5.7}Se_{0.3}$, the T_c further increased to 3.5 K, and bulk nature of superconductivity was confirmed from magnetic shielding volume fraction.

[1]Department of Physics, Tokyo Metropolitan University, 1-1 Minami-Osawa, Hachioji, Tokyo, 192-0397, Japan. [2]University of Yamanashi, 7-32, Miyamae, Kofu, Yamanashi, 400-8511, Japan. Correspondence and requests for materials should be addressed to Y.M. (email: mizugu@tmu.ac.jp)

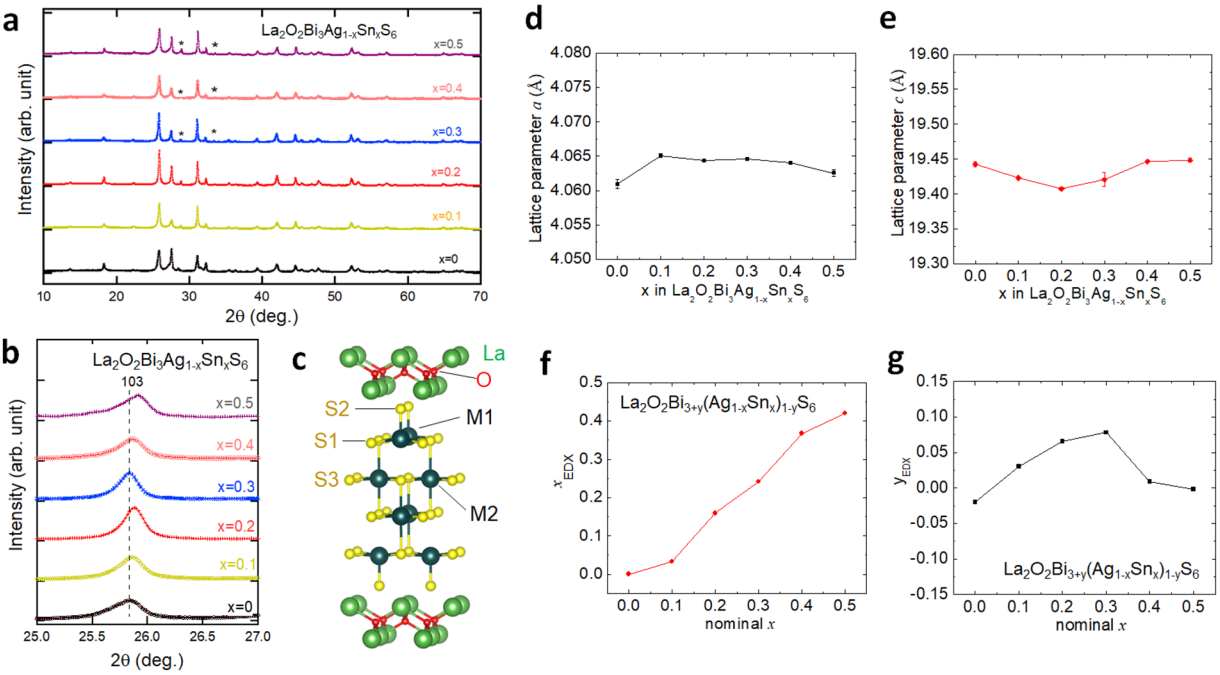

Figure 1. Crystal structure and composition analyses results for $La_2O_2Bi_3Ag_{1-x}Sn_xS_6$ ($x = 0$–0.5). (**a**) Room-temperature XRD pattern for $x = 0$–0.5. The impurity peaks of $La_2Sn_2O_7$ are indicated by asterisks (*). (**b**) XRD pattern near the 103 (Miller index) peak of the tetragonal phase of $La_2O_2Bi_3AgS_6$. (**c**) A schematic image of the crystal structure of $La_2O_2M_4S_6$ (two M sites, M1 and M2, are occupied by Bi, Ag, and Sn in the present system). (**d**,**e**) Lattice parameters of a and c obtained from Rietveld refinements. (**f**,**g**) Nominal composition dependences of compositions (x and y) analyzed by EDX, where x and y are defined as $La_2O_2Bi_{3+y}(Ag_{1-x}Sn_x)_{1-y}S_6$.

Results

Sn substitution effect on structural and physical properties in $La_2O_2Bi_3Ag_{1-x}Sn_xS_6$. Figure 1a displays the room temperature XRD patterns for $La_2O_2Bi_3Ag_{1-x}Sn_xS_6$ ($x = 0$–0.5). All the $La_2O_2Bi_3Ag_{1-x}Sn_xS_6$ samples are crystallized in the tetragonal structure with the space group of $P4/nmm$. An impurity phase of $La_2Sn_2O_7$ was observed for $x = 0.2$–0.5. Figure 1b shows the shift in the 103 peak position, which slightly shifts towards the low angle side for $x = 0.1$. As the Sn concentration increases from $x = 0.2$ to 0.5, the 103 peak shifts towards the higher angle side. The schematic image of the crystal structure of $La_2O_2M_4S_6$ is shown in Fig. 1c. For the $La_2O_2Bi_3Ag_{1-x}Sn_xS_6$ phase, Bi selectively occupies the M1 site, and Sn is expected to substituted for Ag at the M2 site, which was qualitatively confirmed by Rietveld refinements. The evolutions of the lattice parameters by the Sn substitution are shown in Fig. 1d,e. The lattice parameters are $a = 4.061(1)$ Å and $c = 19.445(1)$ Å for $x = 0$ and $a = 4.0648(1)$ Å and $c = 19.48(1)$ Å for $x = 0.1$. The lattice parameter c tends to decrease by Sn substitution for $x = 0$–0.2, and then, it continuously increases with increasing x for $x = 0.2$–0.5. The lattice parameter a increases for the $x = 0.1$, but it tends to decrease with increasing x for higher x. However, the changes in those lattice parameters are small. On the basis of the lattice parameter evolutions, we consider that the Sn substitution does not largely affect the lattice volume, which may be due to smaller ionic radius of Sn^{2+} (93 pm) than that of Ag^{+} (113 pm). The $La_2O_2Bi_3AgS_6$-type structure can be considered as the stacking of a La_2O_2 layer, two BiS_2 layers, and an NaCl-type $AgBiS_2$ layer. In such a layered structure, the unit cell is almost determined by the hardest layer due to the different ionic bonding nature. In this structure, La_2O_2 layer structure is the hardest.

The actual ratio of the metals in the conducting layer (Bi, Ag, and Sn) in the $La_2O_2Bi_3Ag_{1-x}Sn_xS_6$ ($x = 0$–0.5) samples were examined by EDX. The nominal and analyzed values of x are plotted in the Fig. 1f. Although there is slight deviation from the nominal values, the analyzed values of x_{EDX} linearly increases with increasing nominal x. We found that Bi is slightly excess for $x = 0.1$–0.3. Therefore, y parameter with a formula of $La_2O_2Bi_{3+y}(Ag_{1-x}Sn_x)_{1-y}S_6$ was introduced to analyze the Bi concentration. The analyzed values of y_{EDX} are plotted in Fig. 1g. y_{EDX} is higher for $x = 0.1$–0.3 but almost zero for $x = 0$, 0.4, and 0.5. Therefore, we consider that the Bi excess can be ignored in the discussion on the Sn substitution (and Se substitution) effect, and we use the formula $La_2O_2Bi_3Ag_{1-x}Sn_xS_6$ in this paper.

Figure 2a–c show the temperature dependences of magnetic susceptibility ($4\pi\chi$-T) under an applied magnetic field of 10 Oe for $La_2O_2Bi_3Ag_{1-x}Sn_xS_6$ ($x = 0.3$–0.5). The diamagnetic signals in the $4\pi\chi$ curve were observed below 2.2, 2.8, and 2.6 K for $x = 0.3$, 0.4, and 0.5, respectively. A large diamagnetic signal was observed below 2.8 K in the ZFC curve for $x = 0.4$. The shielding value fractions estimated from $4\pi\chi$ (ZFC) at 1.9 K is nearly 20% [See Fig. 2(d).] while it is still not saturated. From the susceptibility results, we consider that Sn substitution is effective to improve the superconducting properties of $La_2O_2Bi_3AgS_6$ but not sufficient to induce bulk superconductivity.

Figure 3 shows the temperature dependences of electrical resistivity from 300 to 0.1 K for $La_2O_2Bi_3Ag_{1-x}Sn_xS_6$ ($x = 0$–0.5). The electrical resistivity at 300 K decreases with increasing Sn concentration up to $x = 0.3$ and

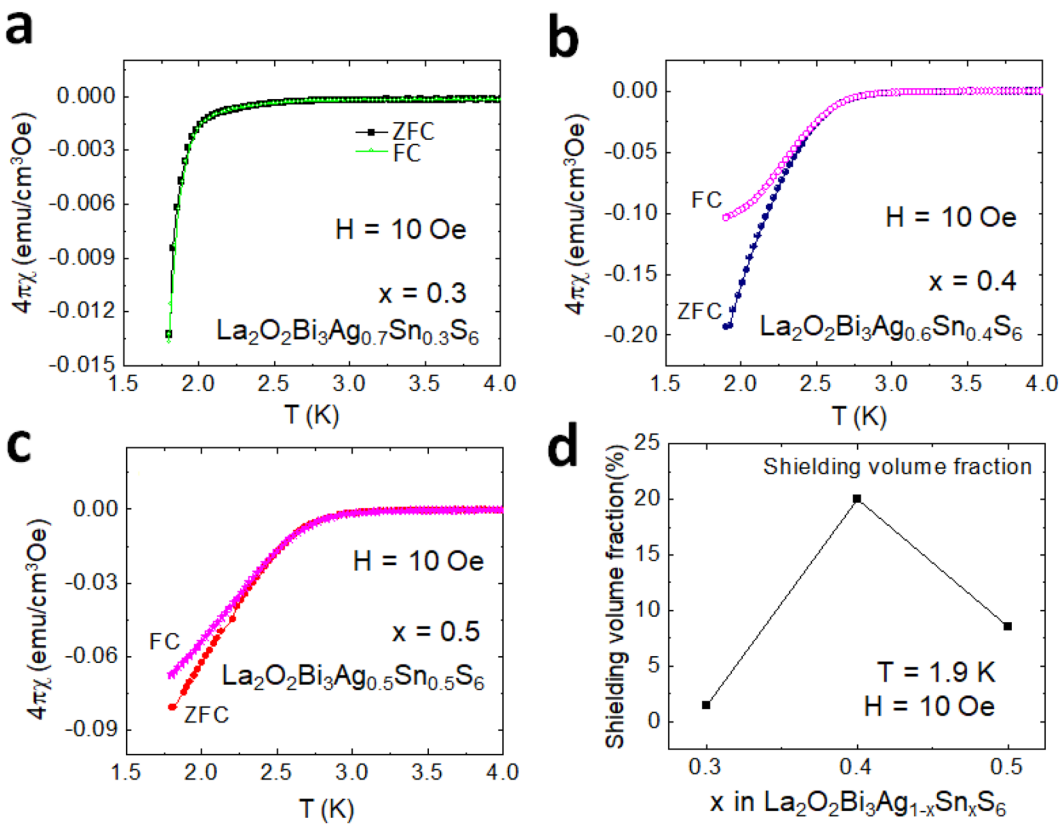

Figure 2. Superconducting properties examined from magnetic susceptibility for $La_2O_2Bi_3Ag_{1-x}Sn_xS_6$ ($x = 0.3$–0.5). (**a**–**c**) Temperature (T) dependences of magnetic susceptibility ($4\pi\chi$) for $x = 0.3$–0.5 measured in the ZFC and FC modes with an applied magnetic field of 10 Oe. (**d**) Sn concentration dependence of the shielding volume fraction estimated using the ZFC data at 1.9 K.

increases again for $x = 0.4$ and 0.5. The normal-state resistivity of the Sn-doped samples changes remarkably. For example, the pure sample ($x = 0$) shows a linear decrease in resistivity on cooling below the anomaly temperature $T^* = 180$ K. A similar behavior was observed up to $x = 0.2$. The resistivity anomaly at T^* appears for $x \leq 0.2$, and the T^* shifts towards the lower temperature side with increasing x. In contrast, the normal-state $\rho(T)$ for $x = 0.3$–0.5 shows an upturn below ~50 K. The anomaly disappears for $x \geq 0.3$. Figure 3g shows the zoomed view of the Figs. 3a–f near the superconducting transition. The T_c clearly increases with increasing Sn concentration in $La_2O_2Bi_3Ag_{1-x}Sn_xS_6$. The highest T_c was achieved for $x = 0.4$, and T_c decreases for a higher substitution with $x = 0.5$.

The room-temperature Seebeck coefficient (S) for $La_2O_2Bi_3Ag_{1-x}Sn_xS_6$ ($x = 0$–0.5) are shown in Fig. 4. The Seebeck coefficient is a good scale for the carrier concentration in BiS_2-based compounds[30]. We observed a slight change in S by Sn substitution. The S in $x = 0.2$–0.4 are almost the same, but that for $x = 0$ and 0.5 are slightly large. This suggests that the carrier concentrations for $x = 0.2$–0.4 are higher than those for $x = 0$ and 0.5. This seems to be related to the evolution of T_c. However, the large change in T_c from 0.6 to 2.3 K between $x = 0.1$ and 0.4 cannot be simply understood by the carrier concentration only.

Figure 5 shows the superconductivity phase diagram of $La_2O_2Bi_3Ag_{1-x}Sn_xS_6$, which shows the interplay between the resistivity anomaly temperature (T^*) and the superconducting transition temperature (T_c^{zero}). The T^* is suppressed by the Sn substitution, and it disappears at $x = 0.3$. The T_c gradually increases with increasing x in $La_2O_2Bi_3Ag_{1-x}Sn_xS_6$. The highest $T_c^{zero} = 2.3$ K is achieved for $x = 0.4$. A lower $T_c^{zero} = 1.9$ K is observed for the highest (solubility-limit) Sn concentration of $x = 0.5$.

Here, we discuss about the possible influence of the presence of the $La_2Sn_2O_7$ impurity to the composition. Due to the change in the impurity amount for $x = 0$–0.5, the actual compositions may deviate from the nominal compositions. Although the Sn concentration to that of Ag was checked by EDX (Fig. 1f), oxygen deficiency in the blocking layer was not checked in this study. However, we consider that oxygen deficiency was not introduced because it is expected to make the structure unstable even if it has been introduced in the $La_2O_2Bi_3AgS_6$-type structure. We have tried to dope electrons by oxygen deficiency or fluorine substitution for the $La_2O_2Bi_3AgS_6$-type structure. However, in the $La_2O_2Bi_3AgS_6$ system, such trials of fluorine substitutions (or oxygen deficiency) resulted in decomposing of the $La_2O_2Bi_3AgS_6$-type structure into $LaO_{1-x}F_xBiS_2$. This indicates that an electron-doped composition with the $La_2O_2Bi_3AgS_6$-type structure cannot be obtained easily due to the competition to the high stability of the $REO_{1-x}F_xBiS_2$-type phase. In addition, oxygen deficiency has not been observed in the $REOBiS_2$ systems.

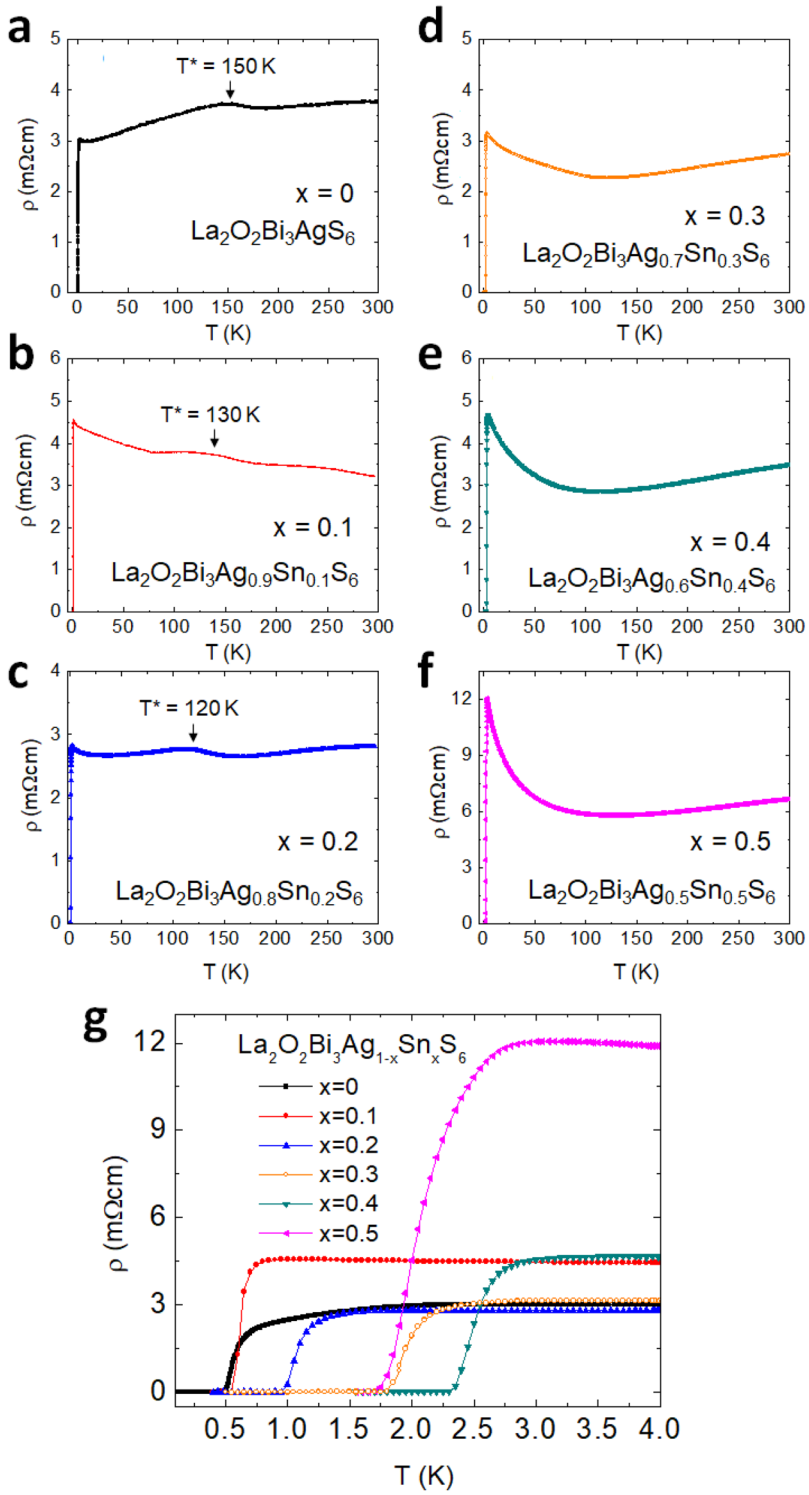

Figure 3. Electrical transport properties for $La_2O_2Bi_3Ag_{1-x}Sn_xS_6$ ($x = 0$–0.5). (**a**–**f**) Temperature dependences of electrical resistivity from 300 to 0.1 K for $x = 0$–0.5. The anomaly temperature in the $\rho(T)$ curves is indicated by T^*. (**g**) The $\rho(T)$ curves in the temperature range of 0.1–4.0 K.

Superconducting properties of Se-doped $La_2O_2Bi_3Ag_{0.6}Sn_{0.4}S_{5.7}Se_{0.3}$. As shown above, the Sn substitution improved the superconducting properties in $La_2O_2Bi_3Ag_{1-x}Sn_xS_6$, and the highest T_c and shielding volume fraction were obtained for $x = 0.4$. In the BiS_2-based compounds, partial Se substitutions for the S site of the superconducting BiS_2 layers have significantly improved the superconducting properties and the bulk characteristics of superconductivity. Therefore, we tried to substitute the S site by Se for the $x = 0.4$ sample. The 5%-Se sample $La_2O_2Bi_3Ag_{0.6}Sn_{0.4}S_{5.7}Se_{0.3}$ was successfully synthesized, but samples with higher Se concentration contained selenide impurity phases. The solubility limit of Se for the S site is around 5%. The composition estimated

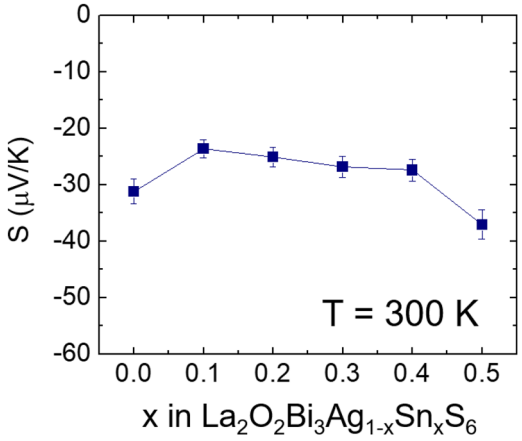

Figure 4. Seebeck coefficient for $La_2O_2Bi_3Ag_{1-x}Sn_xS_6$ ($x = 0$–0.5). The room-temperature Seebeck coefficient (S) is plotted as a function of nominal Sn concentration (x).

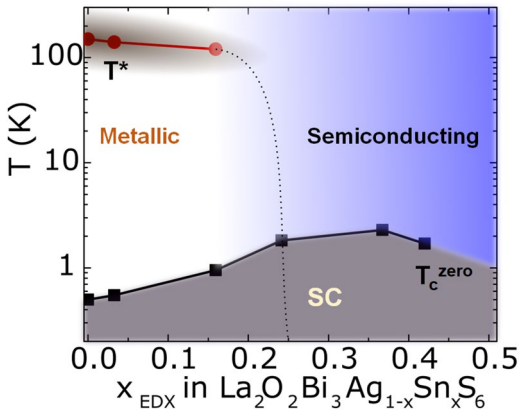

Figure 5. Phase diagram for $La_2O_2Bi_3Ag_{1-x}Sn_xS_6$ ($x = 0$–0.5). The x (Sn concentration estimated from EDX) dependences of T_c^{zero} and T^* are plotted as a function of Sn concentration (x). SC denotes superconductivity.

from the EDX analyses for Bi, Ag, Sn, S, Se elements was $La_2O_2Bi_{3.09}Ag_{0.65}Sn_{0.26}S_{5.73}Se_{0.27}$. Since the obtained composition is close to the nominal formula, we call the sample with the nominal value below.

Figure 6 shows the XRD pattern and the Rietveld refinement result for $La_2O_2Bi_3Ag_{0.6}Sn_{0.4}S_{5.7}Se_{0.3}$. Although two peaks related to the $La_2Sn_2O_7$ impurity phase were observed, other peaks could be refined using the tetragonal ($P4/nmm$) model with a reliability factor R_{wp} of 13.4%. In the refinement, Se was assumed to be substituted for the S1 site. The lattice parameters were $a = 4.0759(2)$ Å and 19.4824(11) Å, which are clearly larger than those of $La_2O_2Bi_3Ag_{1-x}Sn_xS_6$ due to the presence of Se.

Figure 7 displays the superconducting properties of $La_2O_2Bi_3Ag_{0.6}Sn_{0.4}S_{5.7}Se_{0.3}$. As shown in Fig. 7a, a large shielding volume fraction close to 100% was observed. From the resistivity measurements (Fig. 7b), zero resistivity was observed at 3.0 K, and the onset temperature (T_c^{onset}) was 3.5 K; we estimated the temperature where the resistivity becomes almost 90% of normal-state resistivity. Although superconductivity was observed, the $\rho(T)$ curve still shows a semiconducting-like localization at low temperatures. We have measured $\rho(T)$ under magnetic fields up to 9 T. The obtained T_c^{onset} and T_c^{zero} were plotted in Fig. 7d to evaluate the upper critical field H_{c2} and the irreversible field H_{irr}. The $H_{c2}(0)$ was estimated as 2.15 T using the WHH model (Werthamer-Helfand-Hohenberg model)[31]. In addition, from rough estimation with a linear fitting of H_{irr}, the $H_{irr}(0)$ was estimated as 1.0 T.

Discussion

Suppression of resistivity anomaly by the Sn substitution. Here, we discuss the possible origin of the increase in T_c by the Sn substitution. As revealed in the crystal structure part, the lattice parameters were not largely affected by the Sn substitution. Therefore, in-plane chemical pressure amplitude in the Bi-S superconducting plane, which has been revealed as the essential parameter for the emergence of superconductivity in BiS_2-based compounds[24], should not be significantly changed. Therefore, we consider that the in-plane chemical pressure effect is not the origin for the increase in T_c by the Sn substitution. On carrier concentration, the absolute value of the Seebeck coefficient slightly decreases by Sn substitution for $x = 0.1$–0.4, which can be corresponding to the slight increase in electron carriers by Sn substitution. However, the large increase in T_c for $x = 0.4$ may not be understood from the increase in carrier concentration only because the difference in carrier concentration

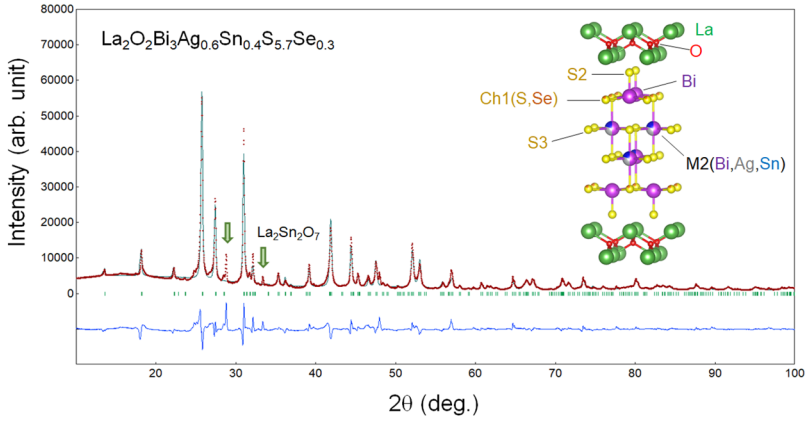

Figure 6. X-ray diffraction analysis for $La_2O_2Bi_3Ag_{0.6}Sn_{0.4}S_{5.7}Se_{0.3}$. XRD pattern and the Rietveld refinement result are shown. The arrows indicate the peaks for the impurity phase $La_2Sn_2O_7$. The inset image shows the crystal structure depicted using the structural parameters obtained from the Rietveld refinement.

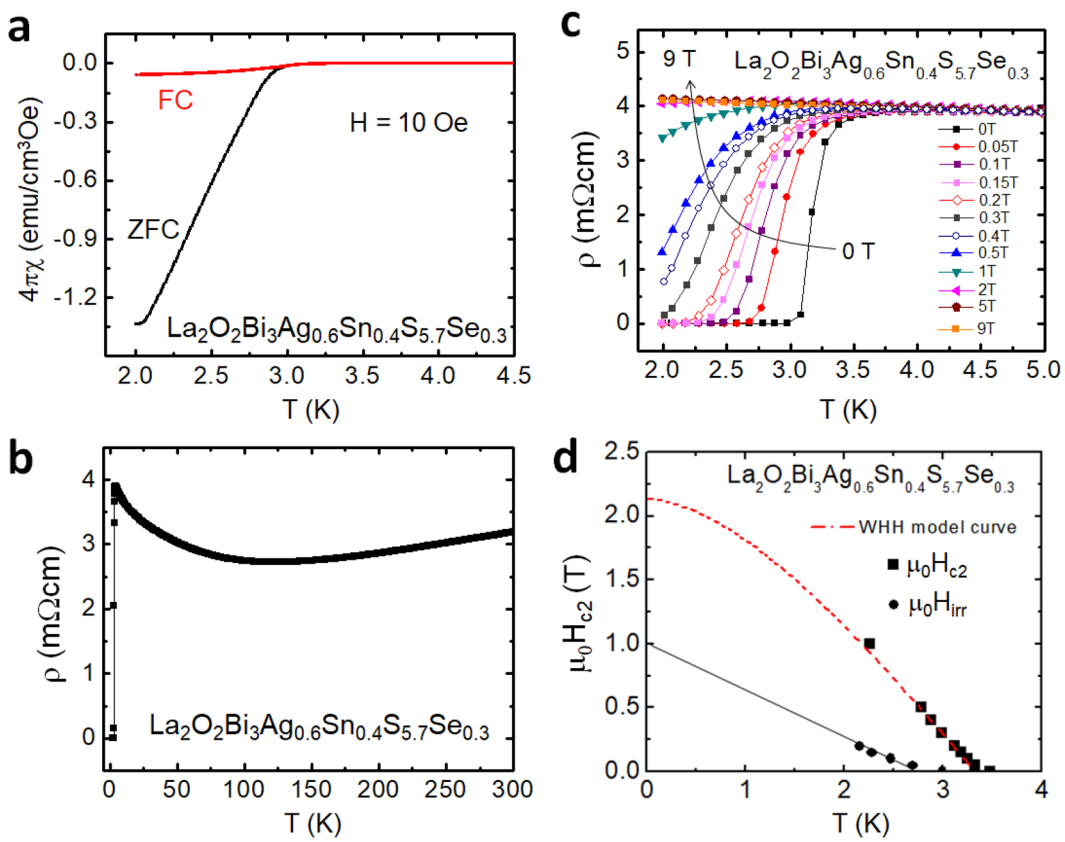

Figure 7. Superconducting properties for $La_2O_2Bi_3Ag_{0.6}Sn_{0.4}S_{5.7}Se_{0.3}$. (**a**) Temperature dependence of magnetic susceptibility. (**b**) Temperature dependence of electrical resistivity [$\rho(T)$]. (**c**) Low-temperature $\rho(T)$ under magnetic fields up to 9T. (**d**) Temperature-magnetic field phase diagram with the upper critical field (H_{c2}) and the irreversible field (H_{irr}).

between $x = 0.1$ ($T_c = 0.6$ K) and $x = 0.4$ ($T_c = 2.3$ K) is expected to be quite small. On the basis of these facts, we briefly mention about the possible relation to the CDW ordering and the possible scenario of the suppression of CDW by Sn substitution in this system. In the ρ-T plots, an anomaly was observed in the $La_2O_2Bi_3Ag_{1-x}Sn_xS_6$ system. A similar feature in the normal-state resistivity has been observed in the $EuFBiS_2$ superconductor ($T_c = 0.3$ K). The origin of the hump was proposed as a CDW transition[29]. We assume that the suppression of the CDW ordering is the origin for the increased T_c in $La_2O_2Bi_3Ag_{1-x}Sn_xS_6$. In addition, the anomaly temperature T^* was shifted to a lower temperature by Sn substitution, and the anomaly disappeared at $x = 0.3$. At around $x = 0.3$ and 0.4, T_c is the maximum. These facts imply that T_c increased by the suppression of T^*. Although we have no

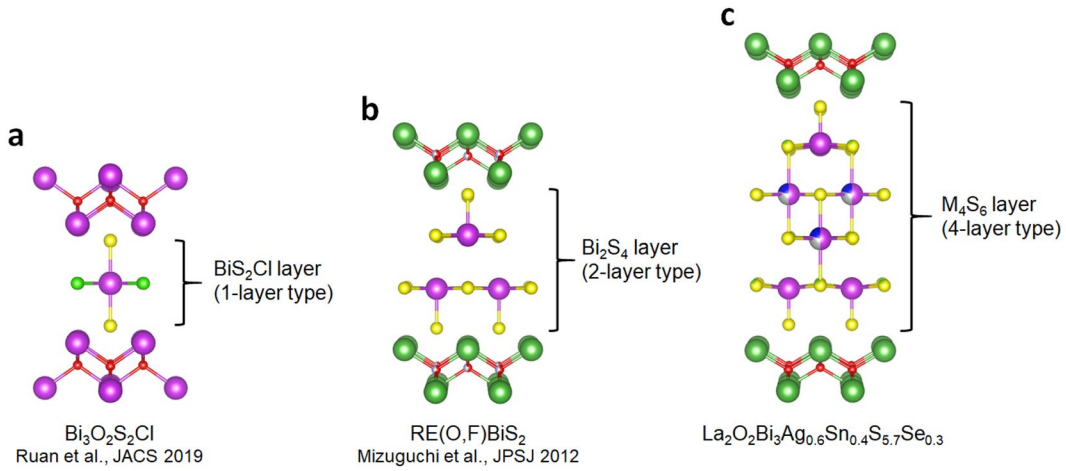

Figure 8. Comparison of crystal structure of typical Bi-based layered compounds with different thickness of superconducting layer. (**a**) Schematic image of the crystal structure of $Bi_3O_2S_2Cl$, which was recently discovered by Ruan *et al.*[34]. In this material, the conducting layer can be regarded as the one-layer-type BiS_2Cl. (**b**) Schematic image of the crystal structure of the typical BiS_2-based superconductor $RE(O,F)BiS_2$. In the series, the conducting layer can be regarded as the two-layer-type Bi_2S_4 bilayer. (**c**) Schematic image of the crystal structure of $La_2O_2Bi_3AgS_6$-type ($La_2O_2M_4S_6$-type) materials whose conducting layer can be regarded as the four-layer-type M_4S_6 layer.

evidence for the CDW states in the $La_2O_2Bi_3Ag_{1-x}Sn_xS_6$ system and the suppression mechanism by the Sn substitution, introduction of randomness at the M2 site may be effective to suppress the charge ordering states.

Bulk superconductivity in $La_2O_2Bi_3Ag_{0.6}Sn_{0.4}S_{5.7}Se_{0.3}$. As shown in the Result part, a partial Se substitution for S induced bulk superconductivity in $La_2O_2Bi_3Ag_{0.6}Sn_{0.4}S_{5.7}Se_{0.3}$. Although the solubility limit of Se for the S site is very low (5%), the lattice parameters clearly changed by the partial Se substitution, and the superconducting properties were significantly improved. Although we refined three models with different Se site (assuming the substitution at the S1, S2, or S3 sites), we could not find the site selectivity of doped Se. However, we expect that the doped Se occupies the Ch1 site in the inset of Fig. 6. In previous reports on the Se substitution in BiS_2-based compounds, the site selectivity of Se at the in-plane site was observed[24,32,33]. According to the relationship between in-plane disorder at the chalcogen site and superconductivity in BiS_2-based systems[16,24], we assume that Se substitution reduced the in-plane disorder at the S1 site and induced bulk superconductivity. Furthermore, the room-temperature Seebeck coefficient for the $La_2O_2Bi_3Ag_{0.6}Sn_{0.4}S_{5.7}Se_{0.3}$ sample was similar to those shown in Fig. 4 ($S = -25\,\mu V/K$). This also suggests that the bulk nature of superconductivity was induced by local structural optimization but not due to changes in carrier concentration.

Since the phases contain Sn in their structure, we have to exclude the possibility of superconductivity of elemental Sn in the examined samples. From XRD, no peaks of Sn was observed. However, amorphous Sn may exist and show superconducting transition. We cannot directly exclude this possibility, but we consider that the bulk superconductivity observed here is not originated from elemental Sn. We have investigated similar Sn substitution effects in the $La_2O_2Bi_2Pb_{2-x}Sn_xS_6$ system. $La_2O_2Bi_2Pb_2S_6$ ($LaOBiPbS_3$) shows an insulating transport property[26,27]. The insulating behavior was not suppressed by Sn substitution, and superconducting transition was not observed for all the examined samples of $La_2O_2Bi_2Pb_{2-x}Sn_xS_6$. This fact may indirectly suggest that the bulk superconductivity observed in the $La_2O_2Bi_3Ag_{0.6}Sn_{0.4}S_{5.7}Se_{0.3}$ sample is not caused by Sn amorphous impurities.

In conclusion, we have reported the emergence of bulk superconductivity in $La_2O_2M_4S_6$-type (four-layer-type) layered oxychalcogenide $La_2O_2Bi_3Ag_{0.6}Sn_{0.4}S_{5.7}Se_{0.3}$. According to the material design strategy shown here, we can further develop related four-layer-type Bi-based layered superconductors. Recently, a new superconductor $Bi_3O_2S_2Cl$ with the one-layer-type Bi-Cl-S superconducting layer was discovered by Ruan *et al.*[34]. In Fig. 8, schematic images of typical one-layer-type (Fig. 8a), two-layer-type (Fig. 8b), and four-layer-type (Fig. 8c) are displayed for comparison. All the materials have the similar RE_2O_2 or Bi_2O_2 blocking layer. By changing the constituent elements in the superconducting layers, the thickness can be changed in this superconductor family. On the basis of these facts, we will be able to design various types of Bi-based layered superconductors with a higher T_c as developed with various Cu-oxide layers in the cuprate family. With such material development with a different type of conducting layer, remarkable changes in superconducting properties can be expected.

Methods

The polycrystalline samples of $La_2O_2Bi_3Ag_{1-x}Sn_xS_6$ with $x = 0$, 0.1, 0.2, 0.3, 0.4, and 0.5 were prepared by a solid-state reaction method. The polycrystalline samples of Se-substituted $La_2O_2Bi_3Ag_{0.6}Sn_{0.4}S_{6-z}Se_z$ with $z = 0.3$ and 0.6 were also prepared by a solid-state reaction method. Powders (or grains) of Bi_2O_3 (99.9%), La_2S_3 (99.9%), Sn (99.99%), and AgO (99.9%) and grains of Bi (99.999%), S (99.99%), and Se (99.99%) with a nominal composition of $La_2O_2Bi_3Ag_{1-x}Sn_xS_{6-z}Se_z$ were mixed in a pestle and mortar, pelletized, sealed in an evacuated quartz tube, and heated in an electric furnace. The heat treatment condition was 725 °C for 15 h for both samples. However, for

$La_2O_2Bi_3Ag_{0.6}Sn_{0.4}S_{6-z}Se_z$, heating the sample to 725 °C in 1 h was needed to suppress the generation of impurity phases. The obtained samples were reground for homogeneity, pelletized, and heated in the same procedure. The phase purity of the prepared samples and the optimal annealing conditions were examined using X-ray diffraction (XRD) with a Cu-K_α radiation. The lattice parameters were determined using the Rietveld method with RIETAN-FP[35]. Schematic image of the crystal structure was drawn using VESTA[36]. The actual composition was analyzed by energy-dispersive X-ray spectroscopy (EDX) on scanning electron microscope TM3030 (Hitachi). The magnetic susceptibility measurements were carried out using a superconducting quantum interference device (SQUID) magnetometer (MPMS-3, Quantum Design). The susceptibility data were taken after both zero-field cooling (ZFC) and field cooling (FC). The temperature dependence of electrical resistivity [$\rho(T)$] was measured by four-terminal method on the Physical Property measurement system (PPMS, Quantum Design). The resistivity measurement down to 0.4 K was measured using a ^{3}He probe platform of PPMS. The ADR system on PPMS was used for resistivity measurements down to 0.1 K. For clarity, we labeled the examined samples with the nominal compositions. The Seebeck coefficient was measured by a four-probe method on ZEM-3 (Advance RIKO) at 300 K.

Data Availability

The datasets generated and analyzed during the current study are available from the corresponding author on reasonable request.

References

1. Bednorz, J. G. & Müller, K. A. Possible high T_c superconductivity in the Ba-La-Cu-O system. *Z. Physik B Condensed Matter* **64**, 189–193 (1986).
2. Kamihara, Y. *et al*. Iron-Based Layered Superconductor $La[O_{1-x}F_x]FeAs$ (x = 0.05−0.12) with T_c = 26 K. *J. Am. Chem. Soc.* **130**, 3296–3297 (2008).
3. Mizuguchi, Y. *et al*. BiS_2-based layered superconductor $Bi_4O_4S_3$. *Phys. Rev. B* **86**(1–5), 220510 (2012).
4. Mizuguchi, Y. *et al*. Superconductivity in Novel BiS_2-Based Layered Superconductor $LaO_{1-x}F_xBiS_2$. *J. Phys. Soc. Jpn.* **81**(1–5), 114725 (2012).
5. Singh, S. K. *et al*. Bulk Superconductivity in Bismuth Oxysulfide $Bi_4O_4S_3$. *J. Am. Chem. Soc.* **134**, 16504–16507 (2012).
6. Demura, S. *et al*. BiS_2-based superconductivity in F-substituted $NdOBiS_2$. *J. Phys. Soc. Jpn.* **82**(1–3), 033708 (2013).
7. Jha, R. *et al*. Synthesis and superconductivity of new BiS_2 based superconductor $PrO_{0.5}F_{0.5}BiS_2$. *J. Supercond. Nov. Magn.* **26**, 499–502 (2013).
8. Jha, R. *et al*. Superconductivity at 5 K in $NdO_{0.5}F_{0.5}BiS_2$. *J. Appl. Phys.* **113**(1–3), 056102 (2013).
9. Xing, J. *et al*. Superconductivity Appears in the Vicinity of an Insulating-Like Behavior in $CeO_{1-x}F_xBiS_2$. *Phys. Rev. B* **86**(1–5), 214518 (2012).
10. Yazici, D. *et al*. Superconductivity of F-substituted $LnOBiS_2$ (Ln = La, Ce, Pr, Nd, Yb) compounds. *Philos. Mag.* **93**(1–8), 673 (2012).
11. Yazici, D. *et al*. Superconductivity induced by electron doping in La1-xMxOBiS2 (M = Ti, Zr, Hf, Th). *Phys. Rev. B* **87**(1–8), 174512 (2013).
12. Lin, X. *et al*. Superconductivity induced by La doping in $Sr_{1-x}La_xFBiS_2$. *Phys. Rev. B* **87**(1–4), 020504 (2013).
13. Mizuguchi, Y. Review of superconductivity in BiS_2-based layered materials. *J. Phys. Chem. Solids* **84**, 34–48 (2015).
14. Mizuguchi, Y. Material Development and Physical Properties of BiS_2-Based Layered Compounds. *J. Phys. Soc. Jpn.* **88**(1–17), 041001 (2019).
15. Usui, H., Suzuki, K. & Kuroki, K. Minimal electronic models for superconducting BiS_2 layers. *Phys. Rev. B* **86**(1–5), 220501 (2012).
16. Mizuguchi, Y. *et al*. Evolution of Anisotropic Displacement Parameters and Superconductivity with Chemical Pressure in BiS_2-Based $REO_{0.5}F_{0.5}BiS_2$ (RE = La, Ce, Pr, and Nd). *J. Phys. Soc. Jpn.* **87**, 023704 (2018).
17. Kotegawa, H. *et al*. Pressure Study of BiS_2-Based Superconductors $Bi_4O_4S_3$ and $La(O,F)BiS_2$. *J. Phys. Soc. Jpn.* **81**(1–4), 103702 (2012).
18. Mizuguchi, Y. *et al*. Stabilization of High-T_c Phase of BiS_2-Based Superconductor $LaO_{0.5}F_{0.5}BiS_2$ Using High-Pressure Synthesis. *J. Phys. Soc. Jpn.* **83**(1–4), 053704 (2014).
19. Wolowiec, C. T. *et al*. Enhancement of superconductivity near the pressure-induced semiconductor–metal transition in the BiS_2-based superconductors $LnO_{0.5}F_{0.5}BiS_2$ (Ln = La, Ce, Pr, Nd). *J. Phys.: Condens. Matter* **25**(1–6), 422201 (2013).
20. Jha, R., Tiwari, B. & Awana, V. P. S. Impact of Hydrostatic Pressure on Superconductivity of $Sr_{0.5}La_{0.5}FBiS_2$. *J. Phys. Soc. Jpn.* **83**(1–4), 063707 (2014).
21. Jha, R., Tiwari, B. & Awana, V. P. S. Appearance of bulk superconductivity under hydrostatic pressure in $Sr_{0.5}RE_{0.5}FBiS_2$ (RE = Ce, Nd, Pr, and Sm) compounds. *J. Appl. Phys.* **117**(1–7), 013901 (2015).
22. Kajitani, J. *et al*. Chemical pressure effect on superconductivity of BiS_2-based $Ce_{1-x}Nd_xO_{1-y}F_yBiS_2$ and $Nd_{1-z}Sm_zO_{1-y}F_yBiS_2$. *J. Phys. Soc. Jpn.* **84**(1–6), 044712 (2015).
23. Hiroi, T. *et al*. Evolution of superconductivity in BiS_2-based superconductor $LaO_{0.5}F_{0.5}Bi(S_{1-x}Se_x)_2$. *J. Phys. Soc. Jpn.* **84**(1–4), 024723 (2015).
24. Mizuguchi, Y. *et al*. In-plane chemical pressure essential for superconductivity in $BiCh_2$-based (Ch: S, Se) layered structure. *Sci. Rep.* **5**(1–8), 14968 (2015).
25. Jha, R. *et al*. Superconductivity in Layered Oxychalcogenide $La_2O_2Bi_3AgS_6$. *J. Phys. Soc. Jpn.* **87**(1–3), 083704 (2018).
26. Sun, Y. L. *et al*. Design and Synthesis of a New Layered Thermoelectric Material $LaPbBiS_3O$. *Inorg. Chem.* **53**, 11125–11129 (2014).
27. Mizuguchi, Y. *et al*. Crystal structure, site selectivity, and electronic structure of layered chalcogenide $LaOBiPbS_3$. *EPL* **119**(p1–p5), 26002 (2017).
28. Hijikata, Y. *et al*. Synthesis, Crystal Structure, and Physical Properties of New Layered Oxychalcogenide $La_2O_2Bi_3AgS_6$. *J. Phys. Soc. Jpn.* **86**(1–4), 124802 (2017).
29. Zhai, H. F. *et al*. Possible Charge-density wave, superconductivity and f-electron valence instability in $EuBiS_2F$. *Phys. Rev. B* **90**(1–9), 064518 (2014).
30. Mizuguchi, Y., Nishida, A., Omachi, A. & Miura, O. Thermoelectric properties of new Bi-chalcogenide layered compounds. *Cogent Phys.* **3**(1–14), 1156281 (2016).
31. Werthamer, N. R., Helfand, E. & Hohenberg, P. C. Temperature and Purity Dependence of the Superconducting Critical Field, H_{c2}. III. Electron Spin and Spin-Orbit Effects. *Phys. Rev.* **147**, 295–302 (1966).
32. Tanaka, M. *et al*. Site selectivity on chalcogen atoms in superconducting La(O,F)BiSSe. *Appl. Phys. Lett.* **106**(1–5), 112601 (2015).
33. Jinno, G. *et al*. Bulk Superconductivity Induced by In-plane Chemical Pressure Effect in $Eu_{0.5}La_{0.5}FBiS_{2-x}Se_x$. *J. Phys. Soc. Jpn.* **85**(1–6), 124708 (2016).
34. Ruan, B. B. *et al*. Superconductivity in $Bi_3O_2S_2Cl$ with Bi-Cl Planar Layers. *J. Am. Chem. Soc.* **141**, 3404–3408 (2019).
35. Izumi, F. & Momma. Three-Dimensional Visualization in Powder Diffraction. *Solid State Phenom.* **130**, 15–20 (2007).
36. Momma, K. & Izumi, F. VESTA: a three-dimensional visualization system for electronic and structural analysis. *J. Appl. Crystallogr.* **41**, 653–658 (2008).

Acknowledgements
We gratefully appreciate O. Miura of Tokyo Metropolitan University for his technical support. This work was financially supported by grants in Aid for Scientific Research (KAKENHI) (Grant Nos 15H05886, 15H05884, 16H04493, 17K19058, 16K05454, and 15H03693) and Advanced Research Program under the Human Resources Funds of Tokyo.

Author Contributions
R.J. synthesized the examined samples. R.J. and Y.M. evaluated the sample qualities and analyzed the crystal structure. R.J., T.D.M., Y.A., M.N. and I.T. measured electrical resistivity and analyzed the data. R.J. and Y.G. measured magnetic susceptibility and Seebeck coefficient. R.J. and Y.M. wrote the manuscript. Y.M. designed the research project.

Additional Information
Competing Interests: The authors declare no competing interests.

Publisher's note Springer Nature remains neutral with regard to jurisdictional claims in published maps and institutional affiliations.